Article

Not peer-reviewed version

Correlative Effects on Nanoplastic Aggregation in Model Extracellular Biofilm Substances Investigated With Fluorescence Correlation Spectroscopy

Tobias Guckeisen , Rozalia Orghici , Silke Rathgeber *

Posted Date: 24 June 2024

doi: 10.20944/preprints202406.1606.v1

Keywords: FCS; Nanoplastics; Nanoparticles; Biofilm; EPS; Aggregation

Article

Correlative Effects on Nanoplastic Aggregation in Model Extracellular Biofilm Substances Investigated with Fluorescence Correlation Spectroscopy

Tobias Guckeisen, Rozalia Orghici † and Silke Rathgeber *

Institute for Integrated Natural Sciences, Physics Department, University of Koblenz, Universitätsstraße 1, 56070 Koblenz, Germany

* Correspondence: rathgeber@uni-koblenz.de

† Current address: Institute for Applied Materials–Electrochemical Technologies, Karlsruhe Institute of Technology, Adenauerring 20b, 76131 Karlsruhe, Germany

Abstract: The increasing micro and nanoplastic pollution is of immense concern. Recent studies show that biofilm substances in contact with nanoplastics play an important role in aggregation and sedimentation of nanoplastics. Consequences of these processes are changes in biofilm formation and stability and changes in transport and fate of pollutants in the environment. Having a deeper understanding of the nanoplastics-biofilm interaction would help to evaluate the risks posed by uncontrolled nanoplastic pollution. These interactions are impacted by environmental changes due to climate change, such as e.g., acidification of surface waters. We apply fluorescence correlation spectroscopy (FCS) to investigate the pH-dependent aggregation tendency of non-functionalized polystyrene (PS) nanoparticles (NPs) due to intermolecular forces with model extracellular biofilm substances. Our biofilm model consists of bovine serum albumin (BSA), which serves as a representative for globular proteins, and the polysaccharide alginate, which is a main component in many biofilms, in solutions containing Na^+ with ionic strength being realistic for fresh water conditions. Biomolecule concentrations ranging from 0.5 g/l up to at maximum 21 g/l are considered. We use non-functionalized polystyrene NPs as representative for mostly negatively charged nanoplastics. BSA promotes NP aggregation through adsorption onto the NPs and BSA mediated bridging. In BSA-alginate mixtures the alginate hampers this interaction, most likely due to alginate-BSA complex formation. Thus, the NP are more stable in the BSA-alginate mixtures compared to solutions containing solely BSA. In most BSA-alginate mixtures and alginate alone, other weaker attractive forces, mainly depletion forces, seem to cause NP aggregation. These forces are not electrostatic in nature and thus are less influenced by the pH-value. At high BSA contents the electrostatic BSA-BSA attraction is not sufficiently screened leading to a destabilization of the NP. This study clearly shows that it is crucial to consider correlative effects between multiple biofilm components to better understand the NP aggregation in the presence of complex biofilm substances. Single component biofilm model systems based on comparing the total organic carbon content of the extracellular biofilm substances, as usually considered, would have led to an misjudgment of the stability towards aggregation. Nevertheless, if the protein content is not too high, a simple model that only depends on polysaccharide concentration could be feasible to predict aggregation under environmental relevant conditions.

Keywords: FCS; nanoplastics; nanoparticles; biofilm; EPS; aggregation

1. Introduction

Biofilms consist of microbial communities that encapsulate themselves in a matrix known as extracellular polymeric substances (EPS). The highly hydrated matrix in a biofilm mainly consist of polysaccharides and proteins and additionally nucleic acids, lipids, and other biopolymers [1]. The matrix provides protection and enables colonization of microorganisms in adverse conditions. It represents a dominant fraction of the reduced-carbon in soils, sediments, and suspended aggregates in ocean and freshwater ecosystems [1]. On the one hand, EPS plays an important role in the environment as a nutrient for the microbiome and is therefore important for the microbial ecology; on the other hand, the microbes produce the EPS and therefore determine its composition.

 doi:10.20944/preprints202406.1606.v1

Plastic pollution, as a result of the worldwide application of plastic products across almost all sectors, is a serious global problem. Especially nanoplastics that originates mostly from breaking down of microplastics is of tremendous concern, because it is believed to have higher toxicity compared to microplastics [3]. This has fueled an increasing interest in nanoplastics research [3], particularly with the focus on the investigation of its interactions with biofilms and biofilm substances present in the natural environment [4]. Interactions between nanoplastics and biofilm substances are known to have strong impact on nanoplastic aggregation [5–8]. Biofilm substances can facilitate nanoparticle (NP) aggregation by bridging from one particle to another and by adsorbing to the NP and thereby changing its surface properties, e.g., its charge or steric hindrance.

Studying the interactions between nanoplastics and biofilms is relevant for a better understanding of its environmental impact. The transport of nanoplastics in the environment can be immensely influenced if the particles are incorporated into biofilms or start aggregating in the presence of EPS substances [9]. For example, when they accumulate in biofilms, nanoplastics can be harmful because they potentially can damage microbial membrane structures, interfere with the diffusion of membrane components [10] and gene expression, and ultimately lead to reduced microbial diversity [2], which is a measure of the variability of the species and a reduction indicates ecotoxic effects. Additionally, they can act as vectors for contaminants, transporting pollutants into the biofilm, such as heavy metals and persistent organic pollutants [5].

However, the biofilm composition, i.e., the proportion of different biofilm substances, is variable and it is yet unclear how this impacts nanoplastics-biofilm interactions. It has been observed that biofilm composition depends on the location within the biofilm [11]. It is also known that changing environmental conditions will also impact biofilm composition. The effects of climate change are altering environmental conditions on a global scale and ecosystem disruption may exacerbate this trend. As an example, different subspecies of *Pseudomonas aeruginosa* can overproduce different components to adapt to varying conditions [12] and it has been seen that biofilm composition is dependent on nutrient availability, temperature and other environmental stress factors, such as acidification of surface waters due to CO_2 emissions, sulfur dioxide or chemical waste pollution [13]. Therefore, it is important to understand how changes in biofilm composition translates into changes in interactions and aggregation with NPs to be able to assess the possible consequences.

Previous investigations on NP aggregation in the presence of natural organic matter (NOM) or exudated biomolecules [6,16–20,28,29] are done via dynamic light scattering (DLS) at low biomolecule concentrations below 0.2 g/l, whereas biofilm density can reach up to 100 g/l [22]. DLS is sensitive to background scattering, therefore measurements at high polymer concentrations are not feasible. For investigations, both monodisperse [6,16–19,21,23–25] and degraded PS nanoparticles [20,26,27] were used as model system for nanoplastics. Some engineered particles are functionalized - mainly with amino and carboxylic acid groups - for electrostatic stabilization and to mimic specific interactions of nanoplastics with natural organic matter. Since polymers containing nitrogen are rare, NP with no modification or carboxylic acid functionalization are given a higher relevance since mechanical degradation with no change in polymer chemistry and photo-thermal oxidation and hydrolysis leading to carboxylic functional groups are the main pathways to nanoplastics in the environment [23].

For the studies NPs were dispersed in natural waters [18,23] or deionized water with different ionic composition [16,17,20,21,26], ionic strength [16,17,20,24–26] and pH-values [6,16,21] simulating fresh [6,21,23] and sea water conditions [16,18,24–27] with a clear focus on the latter. NP stability was characterized in the presence of NOM using natural water or biomass decay products, i.e., refractory humic substances with a focus on the water-soluble components humic and fulvic acid, HA and FA, respectively, [6,17,20,21,23–25,27]. Less attention has been paid to exudated biomacromolecules, like extracellular substances extracted from biofilms [18,19,26] or EPS analogs [16,19], like bovine serum albumin and alginate as representative protein and polysaccharide, respectively.

NOM has generally an overall negative charge, even though some proteins including BSA and humic substances can locally carry positive charges [30,31]. Humic acid (HA) and fulvic acid (FA)

 doi:10.20944/preprints202406.1606.v1

are globular, semi-rigid molecules and are often taken as prevalent example for the hydrophobic fraction of NOM. BSA has a globular shape with protein tertiary structure. It is even more hydrophobic compared to HA and FA. However, BSA, HA, and FA possess local hydrophilic sites. Alginate is a linear, semiflexible, hydrophilic, negatively charged macromolecule [32]. Therefore, it is not surprising that interactions between NP and NOM are complex in nature and include electrostatic and van-der Waals interactions, hydrogen bonding, steric repulsion, ligand formation, hydrophobic-hydrophilic interactions [33,34], and entropy-driven interactions due to conformational changes upon adsorption [35,36]. The interplay between the different interactions depends strongly on the pH-value, salinity and type of ions present in solutions, where a focus was set to the monovalent salt NaCl and the divalent salts $CaCl_2$ and $MgCl_2$ being most relevant in the natural environment.

At low ionic strength, electrostatic interactions predominate. NOM alone or in the presence of monovalent ions (Na^+) has negligible effect on the size distribution of negatively charged NPs [17,21]. Bare or carboxylate functionalized PS. Di-valent (Ca^{2+}, Mg^{2+}) or tri-valent ions (Fe^{3+}) promote aggregation through bridging [17,21,23] without and with NOM as mediator [17]. Barros et al. [19] investigated the interaction of extracted EPS, alginate and BSA i.a. with bare and COOH-functionalized silica particles in deionized water. From an increase in particle diameter and changes in the zeta potentials upon exposure to the biomolecules, the authors deduce that EPS, alginate, and BSA adsorb onto the NPs. In case of the bare silica particles the NPs are stable in the solution with EPS, alginate and BSA. On the carboxylate functionalized particles, adsorption of BSA lowers the surface charge and consequently the electrostatic stabilization, leading to aggregation before sterical stabilization sets in at elevated biomolecule concentrations. For alginate solutions, a similar but much weaker trend is observed. A high density of hydroxyl-groups on the bare silica as well as carboxyl-groups on the functionalized particles might lead to attractive interactions resulting from hydrogen bonding. At ionic strength relevant for sea water conditions, interactions other than repulsive electrostatic interactions become also relevant for PS nanoparticles. NOM, BSA, extracted EPS adsorb on bare and carboxyl-functionalized NPs most likely driven by hydrophobic interactions, hydrogen bonding and/or ligand formation [16,18,20,24,25]. Strong BSA adsorption presumably also originates from structural rearrangements to a more compact globular shape upon adsorption on the NPs leading to a conformation with higher entropy [16]. The hydrophilic alginate exhibits the lowest adsorption tendency [16]. The presence of mono-valent ions (Na^+) can lead first to aggregation due to (partially) charge neutralization [25]. Further increasing the biomolecules concentration results in sterical and electrostatic repulsive forces promoting stabilization effects [16,20,25]. In the presence of di-valent ions (Ca^{2+}) NOM and EPS adsorption can slow down NP aggregation and can reduce the aggregate sizes [18,20], but overall in particular at higher biomolecule concentrations the destabilizing effects due to charge neutralization and bridging are dominating [16,20,24]. From all biomolecules alginate has the strongest destabilization impact which was attributed to the strong ion induced intermolecular bridging between alginate macromolecules resulting in network (gel) formation at high salt contents [16].

In our study, we use model extracellular biofilm substances consisting of protein and polysaccharide at high biomolecule concentrations of 0,5 g/l up to 21 g/l, in contrast to low biomolecule concentrations in previous studies, in solutions containing Na^+ with ionic strength of 10 mmol being realistic for fresh water conditions. We chose bovine serum albumin (BSA) as model protein, since it has representative properties for globular proteins, and alginate as model polysaccharide, which is a component that can be found in many biofilms. Furthermore, we use non-functionalized polystyrene (PS) nanoparticles as representative for mostly negatively charged nanoplastics. We elucidate the effect of different protein-polysaccharide ratios and pH on the NP aggregation in order to derive information about protein, polysaccharide, and NP interactions. Stress factors, i.a. acidification of surface waters due to CO_2 emissions, impact biofilm composition. The pH-value can affect the nanoplastics-polymer interactions since it determines the charge they carry in a given solution. Furthermore, changing the pH also allows for a systematic variation of the electrostatic interactions, giving insight into the role they play in NP aggregation under different conditions. The reduction to a simple model system

 doi:10.20944/preprints202406.1606.v1

together with a systematic variation of the BSA-alginate ratio enables to distinguish the individual contributions of the protein and polysaccharide to the NP aggregation/stabilization. Previous studies did not consider model mixtures and were thus limited in their interpretation by the compositional complexity of the extracted EPS [16,18,19].

To understand how changes in biofilm composition translate into changes in interaction between nanoplastics and biofilm components and how this in turn effects nanoplastic aggregation, we apply fluorescence correlation spectroscopy (FCS). This method is a powerful tool for the investigation of diffusion, aggregation, and other dynamic properties of fluorescent nanoparticles, macromolecules or small molecules [37,38]. In FCS, a small volume with fluorescent species is excited and the fluorescence originating from this volume is detected. The movement of the species through the detection volume is causing fluctuations in fluorescence intensity. Correlation analysis of the intensity fluctuations provides information about the underlying dynamics and concentration of the labeled species. Assuming three-dimensional free diffusion, information about aggregation can be derived from the time dependency of the correlated signal, since the diffusion coefficient and consequently the time spend in the focal volume depends on the particle size. The amplitude of the signal is a direct measure of the number of moving, labelled entities, which increases upon aggregation, while their number decreases. FCS has the advantage to enable measurements at low NP concentrations without compromises in signal strength, since the signal originates from fluctuations in intensity which are amplified at low concentrations. In contrast to DLS, only the labeled species, here NPs, contribute to the signal enabling measurements on higher contents of biopolymer components and mixtures thereof.

Our studies show that in addition to electrostatic interactions, which are important at all concentrations, depletion forces are crucial at higher concentrations. Alginate drives NP aggregation by pH-independent depletion interactions. BSA promotes NP aggregation by adsorption onto the NPs and attractive BSA-BSA interactions, such as hydrogen bonding, hydrophobic interactions and electrostatic interactions resulting from its heterogenous charge distribution, which are in competition with repulsive electrostatic interactions originating from its pH-dependent overall negative net charge at higher pH-values. In protein-polysaccharide mixtures, most likely BSA-alginate complexation leads to a screening of the attractive interactions and consequently, stabilization of the NP solutions compared to solutions containing BSA only. Our study reveals that considering the total organic carbon content of the extracellular biofilm substances can lead to a misestimation of NP stability in complex biofilms, since correlations between the different interactions among proteins, polysaccharides and NP have to be considered. A simple model based on the polysaccharide concentration could be feasible, if the protein concentration is not too high.

2. Materials and Methods

2.1. Material Characterization and Sample Preparation

Reference measurements for FCS were performed on a daily basis by using carboxylate-modified polystyrene (PS) particles. Particles (Fluospheres) were purchased from Molecular Probes, Inc. They have a diameter of 110 nm as cross checked by DLS (Zetasizer, Malvern Panalytical) using the Stokes-Einstein equation (see Equation 6), exhibit an absorption maximum at 505 nm and an emission maximum at 515 nm. The stock solution according to the manufacturer has a concentration of 2 wt% in water (3.6×10^{13} particles /ml = 60 nM). For the reference measurements a concentration of 500 pM was used corresponding to about 2 particles per detection volume. Green fluorescent non-functionalized (plain) and carboxylate-modified PS nanoparticles (NPs) were purchased from RuixiBiotechCo Ltd (article no. R-PGX25) labeled with 4-Chloro-7-nitrobenzofurazan (NBD-Cl) with an excitation and emission maximum of 467 nm and 539 nm, respectively. Here the concentration of the stock solution was 1 wt% (30 nM) in water and the concentration in all FCS measurements was set to 500 pM. For the FCS measurements the non-functionalized (plain) NP were used representative for mostly negatively charged nanoplastics. The carboxylate-modified PS NPs of Ruixibio were measured as a control

 doi:10.20944/preprints202406.1606.v1

with DLS together with the Fluopheres and the non-functionalized NPs. The carboxylate stabilized particles show good agreement between the DLS and FCS measurements and also the Fluospheres correspond well with the supplier's specifications (109 nm). The DLS and FCS measurements of non-functionalized particles differ in size. We attribute this to an increased polydispersity compared to the carboxylate-modified particles as indicated by the higher polydispersity index determined from the DLS measurements. FCS and DLS determine the number averaged and z-averaged sizes, respectively, where the latter puts much stronger weight on large particles.

According to the measured zeta potential all particles are negatively charged under neutral conditions, where the deprotonated carboxyl group contributes to a higher negative charge for the functionalized particles compared to the plain ones. The NP properties are summarized in Table 1.

Table 1. NP properties obtained from dynamic light scattering (DLS) and fluorescence correlation spectroscopy (FCS).

	Fluospheres (COOH)	**R-PGCX25 (COOH)**	**R-PGX25 (plain)**
Diameter supplier	109 nm	100 nm	100 nm
Hydrodynamic diameter (FCS)	reference	105±6 nm	97±7 nm
Hydrodynamic diameter (DLS)	111±2 nm	105±2 nm	124±2 nm
Polydispersity Index (DLS)	0.038	0.031	0.073
Zeta potential (DLS)	-52±4 mV	-51±8 mV	-28±4 mV

BSA was purchased from Biowest (article no. P6154) and alginate (alginic acid sodium salt) of low viscosity (article no. B25266) from Alfa Aesar. The viscosity of alginate is specified by the manufacturer with 30-90 mPas for a 1 % solution in water. Sodium chloride (molecular biology grade) was purchased from VWR (article no. 33614.265) and the water used in all experiments was de-ionized by Seradest SD 4000 with a conductivity < 0.1 µS/cm. The samples with various BSA and alginate content were prepared mixing filtered solution of 10 mM NaCl with appropriate amounts of BSA and alginate from stock solutions having concentrations of 100 g/l and 10 g/l, respectively. The PTFE filters (pore size 0.45 µm) were purchased from Whatman. All pH values were adjusted with HCl from fisher scientific (article no. 10458790) and NaOH from Köhler GmbH (article no. 882219541). NPs were added last, until a final concentration of 500 pM was achieved. Samples were sonicated for 15 min and they remained stable for several hours as shown by control measurements with FCS.

2.2. FCS-Analysis

Movement of fluorescent particles due to Brownian motion through the confocal detection volume induces temporal fluctuations in the fluorescence intensity F(t) at time t, which can be detected by single photon detectors. These fluctuations contain all relevant information about the particle dynamics. From the measured intensity fluctuations, the autocorrelation function can be derived:

$$G(\tau) = \frac{\langle \delta F(t) \delta F(t+\tau) \rangle}{\langle F(t) \rangle^2} \quad (1)$$

$\langle F(t) \rangle$ denotes the time average of the signal, $\delta F(t) = F(t) - \langle F(t) \rangle$ are the fluctuations around the mean value $\langle F(t) \rangle$, and τ is the lag time. The autocorrelation can be exemplified as a measure of self-similarity of the signal. If the fluorescent particles are moving slowly through the detection volume, the signal will stay similar for a longer time, i.e., G(τ) decays more slowly. Assuming a Gaussian shape of the detection volume and three dimensional Brownian diffusion, the following model function can be used to fit FCS curves obtained for solutions containing m populations of diffusing particles with different brightness Q_i, number fraction X_i and diffusion times τ_{Di} (i=1,...,m) [37–39]:

 doi:10.20944/preprints202406.1606.v1

$$G(\tau) = \frac{\sum_{i=1}^{m} Q_i^2 X_i g_i}{N(\sum_{i=1}^{m} Q_i X_i)^2} \tag{2}$$

$$g_i(\tau) = \left(1 + \frac{\tau}{\tau_{Di}}\right)^{-1} \left(1 + \frac{\tau}{S^2 \tau_{Di}}\right)^{-\frac{1}{2}} \tag{3}$$

Here N is the total number of particles in the detection volume and S denotes the aspect ratio of the detection volume, i.e., the ratio of its vertical and lateral diameter measured parallel and perpendicular to the laser beam direction, respectively. For the investigations on partly aggregated samples as conducted here, a model considering two diffusing populations (m=2) was applied. These two populations comprise individual NPs or small aggregates (i=1, diameter d1, volume V1), respectively, and a fraction of large aggregates (i=a, diameter da, volume Va). Assuming that the brightness of an aggregate scales with the number of comprised individual NPs, Equation 2 can be rewritten with $Q_1/Q_a = V_1/V_a = d_1^3/d_a^3$ as follows:

$$G(\tau) = \frac{1 - X_a}{N\left(1 - X_a + X_a(\frac{d_a}{d_1})^3\right)} g_1(\tau) + \frac{X_a(\frac{d_a}{d_1})^6}{N\left(1 - X_a + X_a(\frac{d_a}{d_1})^3\right)} g_a(\tau) \tag{4}$$

Here X_a is the number fraction of large aggregates in the detection volume. g_a and g_1 result from Equation 3 with the diffusion times $\tau_{D,a}$ and $\tau_{D,1}$ of the two populations, respectively. The diffusion time measures the residence time of the particle in the detection volume. When the size of the labeled species is not negligible compared to the size of the detection volume, what is the case here when measuring aggregates of NPs, the following expression for calculating the diffusion time should be used [38,40]:

$$\tau_{D,i} = \frac{{\omega_0}^2 + (\frac{d_i}{2})^2}{4D_i}, i = 1, a \tag{5}$$

where D_i are the diffusion coefficients of the two populations (i=1,a), respectively, and ω_0 is the lateral radius of the detection volume. It should also be noted that Equation 5 is only valid for $d_i \leq 2\omega_0$. The diffusion coefficient can be approximated by the Stokes-Einstein relation strictly valid for spherical particles only:

$$D_i = \frac{k_B \cdot T}{3\pi\eta d_i}, i = 1, a \tag{6}$$

Here k_B is the Boltzmann constant, T the absolute temperature and η the solution viscosity. The aspect ratio S and the lateral radius ω_0 of the detection volume can be determined from reference measurements using spherical particles with known diameter/diffusion coefficient. Reference measurements were done on a daily basis using carboxylate-modified Fluospheres with known diameter (see sample preparation). The diameter of the detection volume was typically ω_0 = 350 nm and the aspect ratio around 11.

Even though the aggregates cannot be assumed to have a spherical shape, Equation 5 and 6 can be taken to calculate the effective hydrodynamic diameter of the aggregates. In Equation 4 polydispersity is not considered, nevertheless, it can also be used in more polydisperse systems such as aggregative systems, yielding an average value of the hydrodynamic diameter [38]. However, absolute values obtained for aggregate dimensions exceeding $2\omega_0 \approx 700$ nm should be taken with precaution. These approximations do not represent any significant restriction for determining the onset of aggregation. The share of aggregates is presented in terms of the volume fraction φ_a instead of the number fraction X_a as it is more sensitive to the onset of aggregation:

 doi:10.20944/preprints202406.1606.v1

$$\varphi_a = \frac{X_a \cdot {d_a}^3}{(1 - X_a){d_1}^3 + X_a {d_a}^3} \tag{7}$$

The FCS curves were fitted using Equation 4. If the χ^2 value of the fit without an aggregate fraction ($X_a = 0$) was equivalent or better than the fit with aggregate fraction, then the fit with fewer parameters ($X_a = 0$) was taken in an Occam's razor approach.

2.3. FCS-Setup

FCS measurements were performed with a home-built setup based on the stand of an inverted Axios Observer Z1 fluorescence microscope using an argon ion laser (LGK 7872 ML, Lasos) for fluorescence excitation at 488 nm. A dichroic mirror (H488 LPXR, 247 AHF) separated the emitted light from the laser excitation. A water immersion objective (LD C-Apochromat 40x, NA 1.1; Zeiss AG) was used to focus and collect the illumination and fluorescence light, respectively. A pinhole (Edmund Optics, d=50 µm) blocks out-of-focus light in the detection path. The fluorescence light is detected by two avalanche photodiodes (Count 100-B, Laser Components) after being split by a 50 % beam splitter (CCM1-BS013/M, Thorlabs). The intensity correlation function was determined by cross-correlating the signal from the two photodiodes, suppressing in this way detector afterpulsing, an artefact that arises from feedback in a single photon detector [41]. For the correlation, a photoncorrelator (DPC 230, Becker & Hickle) operated by the SPCM software was used. FCS curves were calculated by a multiple τ algorithm, within a correlation time window of 10 s. The samples were measured in a circular steel sample container with cover glass at the bottom that can be sealed to avoid evaporation.

All FCS results are the mean of triplicate measurements of at least two independent experiments with freshly prepared samples. The acquisition time was between t_a= 150 - 900 s, depending on the size of the aggregates and the time required for obtaining acceptable statistics. All measurements were performed at a room temperature of 21°C in an air-conditioned room.

2.4. Correction for Viscosity Changes

The time development of the FCS autocorrelation curve depends not only on the diameter of the particles moving through the detection volume but also on viscosity changes due to composition and concentration variations. FCS curves, e.g., will shift to larger diffusion times with increasing particle diameter but also with increasing viscosity because both result in slower diffusion (see Equation 5 and 6). Therefore, the viscosities of the alginate/BSA solutions were measured using an MCR 502 rheometer (Anton Paar) to correct this effect. Measurements were carried out on solutions not containing NPs, since at the NP concentrations considered here, no effect of the NPs on the viscosity of the solutions could be observed. Analogous applies for the globular BSA. Therefore, only the concentration dependent influence of alginate on the viscosity needs to be corrected. Results can be found in a previous publication [42] together with an example for the viscosity change corrections.

3. Results and Discussion

The aggregation of nanoparticles (NPs) in BSA, alginate and BSA-alginate mixtures with a fixed weight ratio of 1:1 were investigated with FCS at different pH-values of 5,7 and 9, respectively. Furthermore, at pH=7 the BSA:alginate weight ratio (1:3, 1:1, 3:1 and 9:1) was changed. The correlation curves of the recorded fluorescence signal were fitted using Equations (4-6) taking into account viscosity changes due to different alginate contents. The resulting volume fraction of aggregates φ_a as well as the hydrodynamic diameters of the smaller sized population d_1 and large aggregates d_a are plotted in Figures 1 and 2 as a function of the BSA, alginate and total biopolymer content, respectively, for the different model biopolymer compositions ranging from 0.5 g/l up to at maximum 21 g/l. Error bars represent the standard error of the mean obtained from evaluating triplicate measurements of two independent experiments on fresh samples.

 doi:10.20944/preprints202406.1606.v1

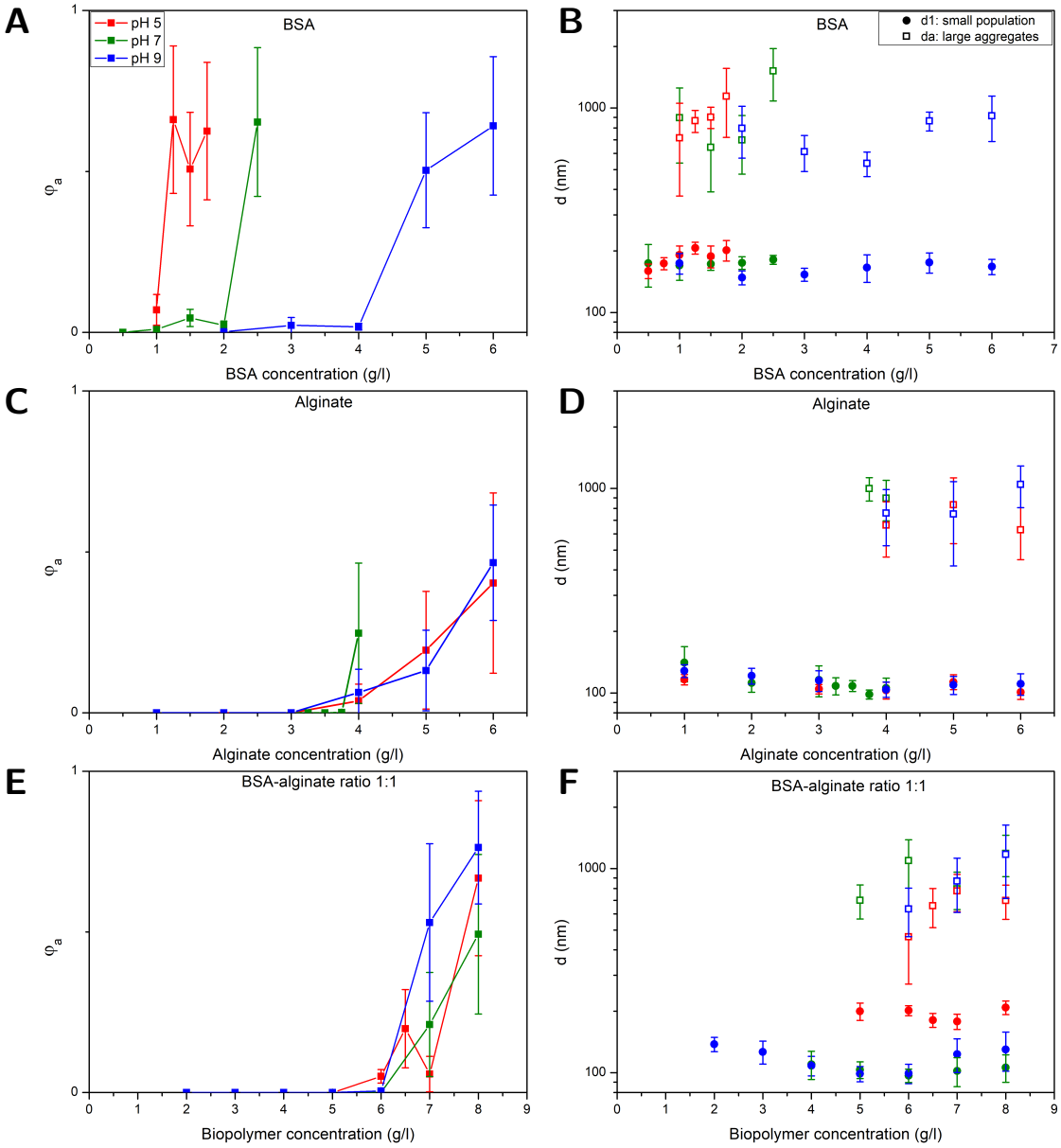

Figure 1. FCS results obtained at different pH-values (buffer: 10 mM NaCl) for PS NPs (⌀ 100 nm) in mixtures with (A+D) BSA, (B+E) alginate and (C+F) BSA and alginate with a fixed BSA-alginate weight ratio of 1:1. Left (A-C): Volume fraction of large aggregates φ_a. Right (D-F): Diameters of the aggregated d_a and smaller sized fraction d_1.

3.1. NP Aggregation in BSA Solutions

Figure 1 (A) shows that the fraction of aggregates φ_a sharply increases with a certain BSA concentration. As pH decreases, the onset of aggregation decreases. The diameters of the two populations, d_1 and d_a, are shown in Figure 1 (B). BSA has a high affinity to the hydrophobic surface of the PS NPs through its hydrophobic units and will cover the NPs to some extent. Independent of the BSA concentration the average diameter of the smaller population is 175±17 nm, which would correspond to a layer thickness of around 38±12 nm if compared to the diameters of the plain particles. The driving force of adsorption of the first protein layer at non-functionalized hydrophobic interfaces is dominated by the hydrophobic interaction [44] and BSA adsorbs readily on a polystyrene (PS)

 doi:10.20944/preprints202406.1606.v1

surface [46–48]. Co-adsorption of positive ions into the NP-BSA contact zone can inhibit the evolution of high electrostatic potentials [49,50]. In addition BSA adsorption is probably driven by structural changes resulting in a higher conformational entropy in the adsorbed state for the protein [16,45]. In multiple layers protein-protein interactions are more important, those can be electrostatic interactions due to the heterogeneous charge distribution of positive and negative patches on the BSA [51,52], but also hydrogen bonding and hydrophobic interactions could be relevant. BSA dimensions are described as an ellipsoid with the dimensions of 14 x 4 x 4 nm [47] and preferably adsorb in a side on orientation on non-functionalized PS surfaces [47].

A layer thickness of 38±12 nm would correspond to about 7-13 layers of BSA which would be considerably more layers than the previously reported mono- or bilayers of BSA on PS surfaces. More likely small aggregates of two or three particles that can't be resolved as an additional species are causing the increase in size. The ability of FCS to resolve small aggregates is limited especially if there is only a small fraction of aggregates present. E.g. a fraction of 10 % can only be resolved under very good signal per particle conditions if the sizes differ at least by a factor of about 2.6 [53]. If the fraction or the signal per particle is lower, here 6 kHz per particle compared to 15 kHz per particle in a more ideal scenario, the size difference has to be even larger. Aggregation of the BSA covered PS NPs is most likely caused by BSA mediated bridging [54]. Despite the negative charge of the PS NPs (see Table 1) and BSA, protein adsorption together with BSA-BSA bridging due to attractive NP-protein and protein-protein interactions, as described above, respectively can induce aggregation. The enhanced aggregation of the NPs at low pH-values can be explained by a decreasing net charge of the BSA and consequently, reduced electrostatic repulsion between the BSA covered NPs. The isoelectric point of BSA is at pH 5 [55], i.e., at this point the BSA molecules carry no net charge and attractive interactions are dominant [51,52]. A lack of electrostatic repulsion between BSA molecules obviously promotes BSA mediated bridging of the NPs which is in accordance with the early onset of NP aggregation at pH=5. At higher pH-values the onset of aggregation is shifted to higher BSA concentrations. This is in line with the increasing absolute value of the net BSA surface potential that changes from 0 mV at pH 5 over -22 mV at pH 7 to -29 mV at pH 9 [56] leading to enhanced electrostatic stabilization of the BSA covered NPs with increasing pH. Within the error bars no significant dependence of the aggregates size on the pH-value and BSA content could be observed.

3.2. NP Aggregation in Alginate Solutions

Figure 1 (C) and (D) display results obtained for φ_a, d_a and d_1 from measurements on alginate-NP mixtures at different pH-values as a function of the alginate concentration. In comparison to the BSA-NP mixtures aggregation sets in between 3 and 4 g/l independent of the pH-value. Alginate carries negatively charged carboxylic acid sides. Unlike BSA, the hydrophilic, negatively charged alginate should not possess significant affinity to the hydrophobic, negatively charged PS particles. Therefore, the NPs should not be covered with alginate, which is consistent with the observation that the diameters obtained for the smaller sized fraction d_1=112±14 nm (see Figure 1 (D)) equals the diameter of 97±7 nm of the pristine NPs within the errors. The driving force for the aggregation arises from a depletion effect, which occurs between large particles in a solution with polymeric substances like alginate. The alginate, which is smaller compared to the NPs, is excluded from gaps between NPs when they approach distances smaller than the alginate size, i.e., on the order of twice the alginate radius of gyration. As a result, the osmotic pressure between polymer (alginate) solution and depletion zone between the NPs leads to an attractive net force pushing the particles together [57–59]. This effect has been already observed for PS particles in both sodium PS sulphonate and alginate solutions [59,60]. Indicated by the absence of a clear pH-effect, electrostatic interactions do not appear to play a major role in alginate-NP mixtures.

 doi:10.20944/preprints202406.1606.v1

3.3. NP Aggregation in BSA-Alginate Mixtures

Figure 1 (E) and (F) depict results for φ_a, d_a and d_1 from studies on NPs in BSA-alginate mixtures with a weight ratio of 1:1 plotted as a function of the overall biopolymer content, i.e., BSA plus alginate. The results are similar to those obtained for NPs in alginate solutions. An increase in the volume fraction of aggregates at alginate concentrations similar to those observed for NP-alginate solutions and no evidence of a pH-effect on aggregation are observed. NPs in BSA solutions aggregate at lower concentrations (between 1 and 2 g/l) than solutions containing BSA-alginate 1:1 mixtures. Thus, although BSA accounts for half of the biopolymer content, there is no indication that attractive BSA-BSA interactions, which were impacted by the pH-dependent net electrostatic charge of the protein in the solutions containing BSA only, drive aggregation. This rather suggests that primarily depletion interactions drive aggregation as in the alginate-NP solutions.

Bridging of NPs by BSA in pristine BSA solutions is based on attractive, electrostatic interactions between positive and negative patches of the protein [51,52]. The negatively charged carboxylic acid sides on alginate can bind to the positively charged protein sides to form BSA-alginate complexes, thus hampering the protein-protein attractive interaction [61]. This also agrees with previous studies of other authors that have shown that alginate and other polyelectrolytes can stabilize protein covered particles [62]. The fact that alginate hinders protein-protein interactions and prevents NP bridging by BSA may indicate that alginate is not completely excluded from the surface, as assumed in classical depletion, but that the entropic or enthalpic penalty for the presence of alginate at the particle surface is insufficient and that there is a finite concentration of alginate, termed weak depletion [63]. However, compared to the NP-alginate mixtures the increase of φ_a in the NP-BSA:alginate mixtures is somewhat steeper and could be caused by BSA mediated bridging once the alginate is (partly) depleted from the NP contact zones.

The diameters of the smaller sized population and aggregated fraction in alginate: BSA 1:1 mixtures are shown in Figure 1 (F). The diameters of the smaller sized population d_1=194±14 nm at pH 5 are considerably larger than those obtained at pH 7 and 9 (d_1=112±14 nm). The d_1-values obtained at pH=5 resemble more the dimension of the species observed in BSA solutions, i.e., most likely small aggregates (see Figure 1 (B)), while values obtained at pH=7 and 9 are similar to the ones obtained for the single NPs in alginate solutions (see Figure 1 (D)). Alginate-BSA complexation presumably hampers the attractive protein-protein interactions at all pH-values investigated. At pH=7 and pH=9 at which BSA carries a negative net charge this might be sufficient to prevent multiple layer formation on the NPs and BSA-BSA bridging. At pH=5 BSA does not carry a net charge reducing repulsive interactions between the BSA enabling that attractive interactions remain to some extent. An intricate interplay of attractive and repulsive interactions determines whether BSA is adsorbed in multiple layers, bridging between particles occurs, or protein aggregates are formed. E.g. many proteins need a critical nucleus for aggregation, so an additional barrier for the formation of this nucleus has to be overcome [64]. Therefore, the formation of multiple BSA layers and BSA-BSA bridging can occur without simultaneous aggregation of BSA, which however cannot be excluded on the basis of the current results.

 doi:10.20944/preprints202406.1606.v1

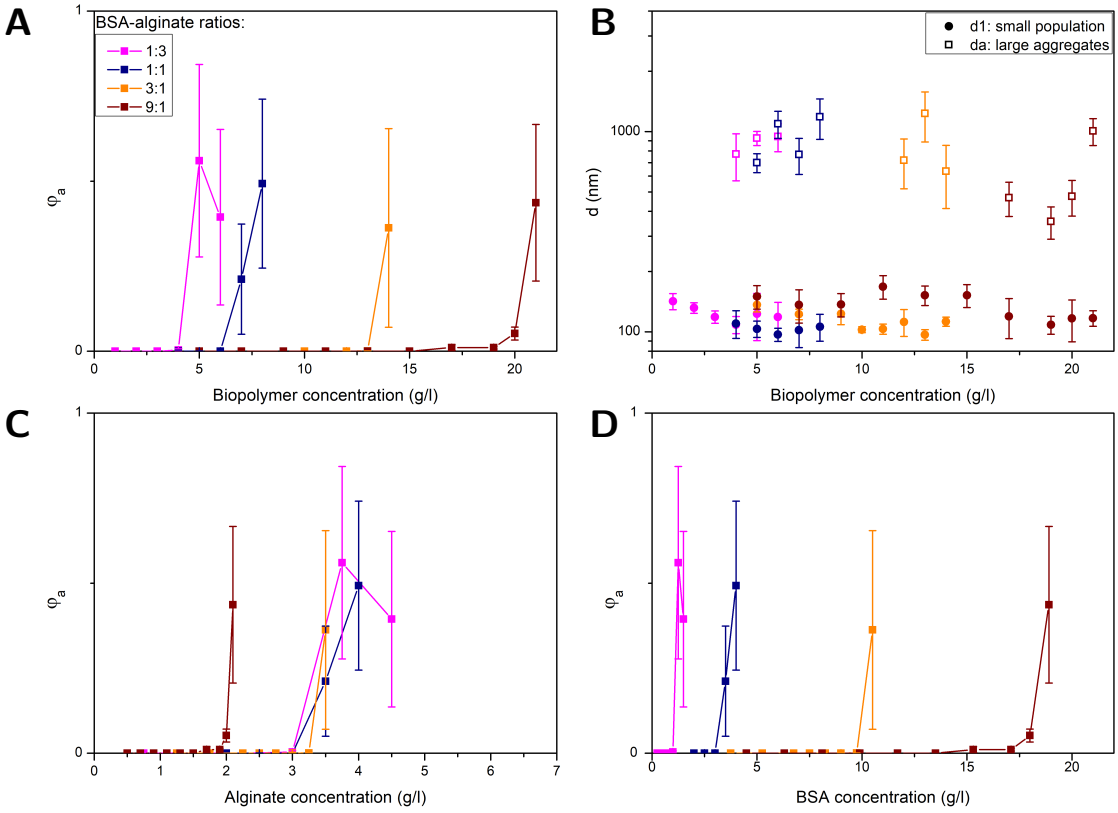

Figure 2. FCS results obtained for PS NPs (100 nm) in solutions with different BSA-alginate weight ratios at pH= 7: Volume fraction of aggregates φ_a versus total biopolymer (BSA + alginate) (A), alginate (C) and BSA (D) content and the diameters of the large aggregates d_a and smaller sized fraction d_1 versus total biopolymer content (B).

Figure 2 (A) and (B) depict results obtained for d_1, d_a and φ_a at pH=7 for different protein-polysaccharide weight ratios (1:3, 1:1, 3:1 and 9:1) as a function of the total biopolymer concentration, i.e., alginate plus BSA. Up to a BSA-alginate weight ratio of (3:1) the diameters d_1=114±14 nm obtained for the smaller sized fraction (see Figure 2 (B)) are comparable to the results obtained for alginate-NP solutions. The values approximately correspond to the dimensions of single NPs. There are no indications for multiple BSA -layer adsorption nor BSA-BSA bridging. In the BSA-alginate (9:1) mixture BSA-BSA interaction is most likely not sufficiently screened by the alginate leading to slightly increased dimensions of about d_1=136±21 nm. The biofilm substances and EPS are often measured without differentiation between protein and polysaccharides as total organic carbon (TOC) content. The combined biopolymer concentration here reflects what is encountered when only TOC is considered. Figure 2 (C) and (D) compare the results obtained for φ_a shown in Figure 2 (A) as a function of the biopolymer content, now plotted versus alginate and BSA concentration, respectively. The concentration at which aggregation starts increases with higher protein portion since alginate is hampering the BSA-BSA interaction. BSA is then contributing only to the biopolymer concentration, but does not cause aggregation.

While aggregation starts always at different BSA concentrations (see Figure 2 (D)), aggregation starts for BSA: alginate weight ratios of 1:3, 1:1 and 3:1 at the same alginate concentration, the value being comparable to one obtained for NPs in pure alginate solutions. In these mixtures the alginate is mainly causing the aggregation by depletions interactions. Thus, a model that only considers the alginate concentration could be useful as long as the protein-polysaccharide ratio is not too high. At high BSA contents the attractive BSA-BSA interaction is not efficiently screened by the alginate shifting

 doi:10.20944/preprints202406.1606.v1

the aggregation threshold to lower alginate concentrations. However, protein-polysaccharide ratios of 9:1 and more actually occur demanding more complex models. A simple model based solely on alginate or BSA would lead to a misjudgment of the aggregation behavior, i.e., overestimation or underestimation of the NP stability, respectively. These results emphasize the importance of knowing the composition of biofilm substances rather than just measuring the total organic carbon content.

4. Conclusions

FCS was used to investigate the aggregation of nanoplastics in model extracellular biofilm substances consisting of the partly positively charged and partly hydrophobic protein BSA and the anionic polysaccharide alginate, and mixtures thereof, at selected pH-values. It has been shown that both biofilm components influence the aggregation of negatively charged, hydrophobic PS NPs in a significant and specific way and that correlative effects originating from the presence of both components cannot be neglected. Alginate drives NP aggregation by pH-independent depletion interactions. Attractive BSA-BSA interactions, i.e., electrostatic interactions between positive and negative patches of the protein, hydrogen bonding and hydrophobic interactions, are responsible for aggregation of BSA covered PS particles in pure BSA solutions. Repulsive electrostatic BSA-BSA interactions due to the pH-dependent negative net charge of BSA reduces the aggregation tendency of the NPs at pH-values above 5, i.e., the isoelectric point of BSA. In the presence of alginate, these interactions are (partly) screened, most likely due to alginate-BSA complex formation, and depletion forces become more relevant for NP aggregation. For a certain range of alginate: BSA ratios the aggregation of the NPs is mainly driven by depletion interactions. However, at high BSA contents the attractive BSA-BSA interaction is not sufficiently screened leading to the aggregation behavior not sufficiently reproduced by a single component model, neither pure alginate nor BSA. Furthermore, the present work demonstrates that a model for biofilm substances consisting of a single component, that is based on comparing the total organic carbon content of the extracellular biofilm substances -which is a path often followed for the sake of simplicity- would have led to an underestimation of the stability towards aggregation. However, for a certain range of protein: polysaccharide ratios (here up to 3:1) a simple model based on comparing the polysaccharide contents instead of the total biopolymer concentration might be feasible to predict NP aggregation under environmental conditions. Therefore, it is of utmost importance to know the composition of biofilm substances including protein and polysaccharide fraction to better understand the NP stability in the presence of complex biofilm substances, in particular if results obtained for different systems are compared.

Author Contributions: Investigation, writing-original draft preparation T.G.; conceptualization, formal analysis T.G., S.R.; methodology T.G., R.O., S.R.; writing-review, supervision R.O., S.R.; funding acquisition S.R. All authors have read and agreed to the published version of the manuscript.

Funding: This research was supported by The 'Forschungsinitiative Rheinland-Pfalz'.

Institutional Review Board Statement: Not applicable.

Data Availability Statement: Data is available on request.

Conflicts of Interest: The authors declare no conflicts of interest.

Abbreviations

The following abbreviations are used in this manuscript:

FCS	Fluorescence correlation spectroscopy
PS	Polystyrene
NP(s)	Nanoparticle(s)
BSA	Bovine serum albumin
EPS	Extracellular polymeric substances
NOM	Natural organic matter

 doi:10.20944/preprints202406.1606.v1

HA	Humic acid
FA	Fulvic acid
TOC	Total organic carbon

References

1. Flemming, H.C.; Wingender, J. The biofilm matrix. *Nat. Rev. Microbiol.* **2010**, *8*, 623–633.
2. Miao, L.; Guo, S.; Liu, Z.; Liu, S.; You, G.; Qu, H. et al. Effects of Nanoplastics on Freshwater Biofilm Microbial Metabolic Functions as Determined by BIOLOG ECO Microplates. *Int. J. Environ. Res. Public Health* **2019**, *16(23)*, 4639.
3. Wang, J.; Zhao, X.; Wu, F.; Niu, L.; Tang, Z.; Liang, W. et al. Characterization, occurrence, environmental behaviors, and risks of nanoplastics in the aquatic environment: Current status and future perspectives. *Fundamental Research* **2021**, *1(3)*, 317–328.
4. Deschênes, L.; Ells, T. Bacteria-nanoparticle interactions in the context of nanofouling. *Adv. Colloid Interface Sci.* **2020**, *277*, 102106.
5. Alimi, O.S.; Budarz, J.F.; Hernandez, L.M.; Tufenkji, N. Microplastics and Nanoplastics in Aquatic Environments: Aggregation, Deposition, and Enhanced Contaminant Transport. *Environ. Sci. Technol.* **2018**, *52*, 1704–1724.
6. Oriekhova, O.; Stoll, S. Heteroaggregation of nanoplastic particles in the presence of inorganic colloids and natural organic matter. *Environ. Sci. Nano* **2018**, *5*, 792–799.
7. Walker, H.W.; Bob, M.M. Stability of particle flocs upon addition of natural organic matter under quiescent conditions . *Water Res.* **2001**, *35(4)*, 875–882.
8. Ge, Z.; Lu, X. Impacts of extracellular polymeric substances on the behaviors of micro/nanoplastics in the water environment. *Environ. Poll.* **2023**, *338*, 122691.
9. Corsi, I.; Bergami, E.; Grassi, G. Behavior and Bio-Interactions of Anthropogenic Particles in Marine Environment for a More Realistic Ecological Risk Assessment. *Front. Environ. Sci.* **2020**, *8*, 60.
10. Rossi, G.; Barnoud, J.; Monticelli, L. Polystyrene Nanoparticles Perturb Lipid Membranes. *J. Phys. Chem. Lett.* **2014**, *5(1)*, 241–246.
11. Ahimou, F.; Semmens, M.J.; Haugstad, G.; Novak, P.J. Effect of Protein, Polysaccharide, and Oxygen Concentration Profiles on Biofilm Cohesiveness. *Appl. Environ. Microbiol.* **2007**, *73(9)*, 2905–2910.
12. Mann, E.E.; Wozniak, D.J.L. Pseudomonas biofilm matrix composition and niche biology. *FEMS Microbiol. Rev.* **2012**, *36(4)*, 893–916.
13. Moryl, M.; Kaleta, A.; Strzelecki, K.; Rozalska, S.; Rozalski, A. Effect of nutrient and stress factors on polysaccharides synthesis in Proteus mirabilis biofilm. *Acta Biochim. Pol.* **2014**, *61(1)*, 133–139.
14. Gounani, Z.; Asadollahi, M.A.; Pedersen, J.N.; Lyngso, J.; Pederson, J.S.; Arpanaei, A. et al. Mesoporous silica nanoparticles carrying multiple antibiotics provide enhanced synergistic effect and improved biocompatibility. *Colloids Surf. B Biointerfaces* **2019**, *175*, 498–508.
15. Natan, M.; Banin, E. From Nano to Micro: using nanotechnology to combat microorganisms and their multidrug resistance. *FEMS Microbiol. Rev.* **2017**, *41*, 302–322.
16. Liu, Y.; Huang, Z.; Zhou, J.; Tang, J.; Yang, C.; Chen, C. et al. Influence of environmental and biological macromolecules on aggregation kinetics of nanoplastics in aquatic systems. *Water Res.* **2020**, *186*, 116316.
17. Cai, L.; Hu, L.; Shi, H.; Ye, J.; Zhang, Y.; Kim, H. Effects of inorganic ions and natural organic matter on the aggregation of nanoplastics. *Chemosphere* **2018**, *197*, 142–151.
18. Grassi, G.; Gabellieri, E.; Cioni, P.; Paccagnini, E.; Faleri, C.; Lupetti, P. et al. Interplay between extracellular polymeric substances (EPS) from a marine diatom and model nanoplastic through eco-corona formation. *Sci. Total Environ.* **2020**, *725*, 138457.
19. Barros, C.H.N.; Fulaz, S.; Vitale, S.; Casey, E.; Quinn, L. Interactions between functionalised silica nanoparticles and Pseudomonas fluorescens biofilm matrix: A focus on the protein corona. *PLoS ONE* **2020**, *15(7)*, e0236441.
20. Yu, S.; Shen, M.; Li, S.; Fu, Y.; Zhang, D.; Liu, H. et al. Aggregation kinetics of different surface-modified polystyrene nanoparticles in monovalent and divalent electrolytes. *Environ. Pollut.* **2019**, *255*, 113302.

 doi:10.20944/preprints202406.1606.v1

21. Zhang, F.; Wang, Z.; Wang S.; Fang, H.; Wang, D. Aquatic behavior and toxicity of polystyrene nanoplastic particles with different functional groups: Complex roles of pH, dissolved organic carbon and divalent cations. *Chemosphere* **2019**, *228*, 195–203.
22. Bishop, P.L.; Zhang, T.C.; Fu, Y. Effects of biofilm structure, microbial distributions and mass transport on biodegradation processes. *Water Sci. Technol.* **1995**, *31(1)*, 143–152.
23. Song, Z.; Yang, X.; Chen, F; Zhao, F; Zhao, Y; Ruan, L. et al. Fate and transport of nanoplastics in complex natural aquifer media: Effect of particle size and surface functionalization. *Sci. Total Environ.* **2019**, *669*, 120–128.
24. Tallec, K.; Blard, O.; Gonzales-Fernandez, C.; Brotons, G; Berchel, M; Soudant, P. et al. Surface functionalization determines behavior of nanoplastic solutions in model aquatic environments. *Chemosphere* **2019**, *225*, 639–646.
25. Wu, J.; Jiang, R.; Lin, W.; Ouyang, G. Effect of salinity and humic acid on the aggregation and toxicity of polystyrene nanoplastics with different functional groups and charges. *Environ. Pollut.* **2019**, *245*, 836–843.
26. Mao, Y.; Li, H.; Huangfu, X.; Liu, Y.; He, Q. Nanoplastics display strong stability in aqueous environments: Insights from aggregation behaviour and theoretical calculations. *Environ. Pollut.* **2020**, *258*, 113760.
27. Xu, Y.; Ou, Q.; He, Q.; Wu, Z.; Ma, J.; Huangfu, X. Influence of dissolved black carbon on the aggregation and deposition of polystyrene nanoplastics: Comparison with dissolved humic acid. *Water Res.* **2021**, *196*, 117054.
28. Pradel, A.; Catrouillet, C.; Gigault, J. The environmental fate of nanoplastics: What we know and what we need to know about aggregation. *NanoImpact* **2023**, *29*, 100453.
29. Cid-Samamed, A.; Diniz, M.S. Recent Advances in the Aggregation Behavior of Nanoplastics in Aquatic Systems. *Int. J. Mol. Sci* **2023**, *24*, 13995.
30. Buffle, J.; Wilkinson, K.J.; Stoll, S.; Filella, M.; Zhang, J. A Generalized Description of Aquatic Colloidal Interactions: The Three-colloidal Component Approach. *Environ. Sci. Technol.* **1998**, *32*, 2887–2899.
31. Wheeler, K.E.; Chetwynd, A.J.; Fahy, K.M.; Hong, B.S.; Tochihuitl, J.A.; Foster, L.A. et al. Environmental dimensions of the protein corona. *nature nanotechnol.* **2021**, *16*, 617–629.
32. Moe, S.T.; Draget, K.I.; Skjåk-Bræk, G.; Smidsrød, O. Alginates. In *Food polysaccharides and their application*; Dekker: New York, United States, 1995; pp. 289–334.
33. Grillo, R.; Rosa, A.H.; Fraceto, L.F. Engineered nanoparticles and organic matter: A review of the state-of-the-art. *Chemosphere* **2015**, *119*, 608–619.
34. Hu, B.; Liu, R.; Liu, Q.; Lin, Z.; Shi, Y.; Li, J. et al Engineering surface patterns on nanoparticles: new insights into nano-bio interactions. *J. Mater. Chem. B* **2022**, *10*, 2357–2383.
35. Kopac, T. A Protein corona, understanding the nanoparticle–protein interactions and future perspectives: A critical review. *Int. J. Biol. Macromolecules* **2021**, *169*, 290–301.
36. Saptarshi, S.; Duschl, A.; Lopata, A.L. Interaction of nanoparticles with proteins: relation to bio-reactivity of the nanoparticle. *J. Nanobiotechnol.* **2013**, *11*, 26.
37. Ries, J.; Schwille, P. Fluorescence correlation spectroscopy. *Bioessays* **2012**, *34(5)*, 361–368.
38. Koynov, K.; Butt, H.J. Fluorescence correlation spectroscopy in colloid and interface science. *Curr. Opin. Colloid Interface Sci.* **2012**, *17(6)*, 377–387.
39. PicoQuant, Practical manual for fluorescence microscopy techniques, Fluorescence correlation spectroscopy (FCS). URL: https://www.picoquant.com/images/uploads/page/files/17319/5_fcs.pdf (accessed 18-03-2024).
40. Starchev, K.; Zhang, J.; Buffle, J. Applications of Fluorescence Correlation Spectroscopy— Particle Size Effect. *J. Colloid Interface Sci.* **1998**, *203(1)*, 189–196.
41. Zhao, M.; Jin, L.; Chen, B.; Ding, Y.; Ma, H.; Chen, D. Afterpulsing and its correction in fluorescence correlation spectroscopy experiments. *Appl. Opt.* **2003**, *42(19)*, 4031–6.
42. Guckeisen, T.; Orghici, R.; Rathgeber, S. Probing the tendency for aggregation of nanoplastics in model extracellular biofilm substances with fluorescence correlation spectroscopy. *Single Molecule Spectroscopy and Superresolution Imaging XVI. Proc. of SPIE* **2023**, *12386*, 1238606.
43. Beragoui, M.; Chadlia, A.; Khalfaoui, M.; Enciso, E.; Torralvo, M.J.; Duclaux, L. et al. Bovine serum albumin adsorption onto functionalized polystyrene lattices: A theoretical modeling approach and error analysis. *Prog. Theor. Exp. Phys.* **2015**, *2015(3)*, 033J01.

 doi:10.20944/preprints202406.1606.v1

44. Yoon, J.Y.; Kim, J.H.; Kim, W.S. The relationship of interaction forces in the protein adsorption onto polymeric microspheres. *Colloids Surf. A Physicochem. Eng. Asp.* **1999**, *153*, 413–419.
45. Norde, W.; Anusiem, A.C.I. Adsorption, desorption and re-adsorption of proteins on solid surfaces. *Coll. Surf.* **1992**, *66*, 73–80.
46. Zsom, R.L.J.; Dependence of preferential bovine serum albumin oligomer adsorption on the surface properties of monodisperse polystyrene latices. *J. Colloid Interface Sci.* **1986**, *111(2)*, 434–445.
47. Wangkam, T.; Yodmongkol, S.; Disrattakit, J.; Sutapun, B.; Amarit, R.; Somboonkaew, A. et al. Adsorption of bovine serum albumin (BSA) on polystyrene (PS) and its acid copolymer. *Curr. Appl. Phys.* **2012**, *12(1)*, 44–52.
48. Rabe, M.; Verdes, D.; Seeger, S. Understanding protein adsorption phenomena at solid surfaces. *Adv. Colloid Interface Sci.* **2011**, *162*, 87–106.
49. Dulm, P. V.; Norde, W.; Lyklema, J. Ion participation in protein adsorption at solid surfaces. *J. Colloid Interface Sci.* **1981**, *82(1)*, 77–82.
50. Elgersma, A.V.; Zsom, R.L.J.; Norde, W.; Lyklema, J. The adsorption of bovine serum albumin on positively and negatively charged polystyrene latices. *J. Colloid Interface Sci.* **1990**, *138(1)*, 145–156.
51. Grant, M.L.; Nonuniform Charge Effects in Protein-Protein Interactions. *J. Phys. Chem. B* **2001**, *105(14)*, 2858–2863.
52. Kubiak-Ossowska, K.; Jachimska, B.; Mulheran, P. How Negatively Charged Proteins Adsorb to Negatively Charged Surfaces: A Molecular Dynamics Study of BSA Adsorption on Silica. *J. Phys. Chem. B* **2016**, *120*, 10463–10468.
53. Meseth, U.; Wohland, T.; Rigler, R.; Vogelc H. Resolution of Fluorescence Correlation Measurements. *Biophys. J.* **1999**, *76*, 1619–1631.
54. Chen, K.; Xu, Y.; Rana, S.; Miranda, O.R.; Dubin, P.L.; Rotello, V.M. et al. Electrostatic Selectivity in Protein-Nanoparticle Interactions. *Biomacromolecules* **2011**, *12*, 2552–2561.
55. Guckeisen, T.; Hosseinpour, S.; Peukert, W. Isoelectric Points of Proteins at the Air/Liquid Interface and in Solution. *Langmuir* **2019**, *35*, 5004–5012.
56. Salis, A.; Boström, M.; Medda, L.; Cugia, F.; Barse, B.; Parsons, D.F. et al. Measurements and Theoretical Interpretation of Points of Zero Charge/Potential of BSA Protein. *Langmuir* **2011**, *27*, 11597–11604.
57. Mao, Y.; Cates, M.E.; Lekkerkerker, H.N.W. Depletion force in colloidal systems. *Physica A* **1995**, *222*, 10–24.
58. Smith, N.J.; Williams, P.A. Depletion Flocculation of Polystyrene Latices by Water-soluble Polymers. *J. Chem. Soc., Faraday Trans.* **1995**, *91(10)*, 1483–1489.
59. Sharma, A.; Tan, S.N.; Walz, J.Y. Effect of Nonadsorbing Polyelectrolytes on Colloidal Interactions in Aqueous Mixtures. *J. Colloid Interface Sci.* **1997**, *191*, 236–246.
60. Bondy, C.; The creaming of rubber latex. *Trans. Faraday Soc.* **1939**, *35*, 1093–1108.
61. Zhao, Y.; Carvajal, M.T.; Harris, M.T. Interactions between bovine serum albumin and alginate: An evaluation of alginate as protein carrier. *J. Coll. Int. Sci.* **2009**, *332(2)*, 1345–353.
62. Sabet, S.; Seal, C.K.; Swedlund, P.J.; McGillivray, D.J. Depositing alginate on the surface of bilayer emulsions. *Food Hydrocoll.* **2020**, *100*, 105385.
63. Garcia, A.G.; Nagelkerke, M.; Tuinier, R.; Vis, M. Polymer-mediated colloidal stability: on the transition between adsorption and depletion. *Adv. Colloid Interface Sci.* **2020**, *275*, 102077.
64. Auer, S.; Dobson, M.D.; Vendruscolo, M. Characterization of the nucleation barriers for protein aggregation and amyloid formation. *HFSP J.* **2007**, *1(2)*, 137–146.
65. McSwain, B.S.; Irvine, R.L.; Hausner, M.; Wilderer, P.A. Composition and Distribution of Extracellular Polymeric Substances in Aerobic Flocs and Granular Sludge. *Appl. Environ. Microbiol.* **2005**, *71(2)*, 1051–1057.